Nano Research

Open Access

Research Article

A damping and adhesive hydrogel electrode for continuous high-fidelity dynamic electrophysiological monitoring and human–machine interaction

Pengcheng Zhu, Yitao Zhang, Aobin Wu, Yunxiang Feng, Yiming Liu, Mengjuan Niu, Ningning Han, Yuyang Lin, Zhifeng Pan, and Yanchao Mao ✉

Key Laboratory of Materials Physics of Ministry of Education, School of Physics, Zhengzhou University, Zhengzhou 450001, China

Cite this article: *Nano Research*, **2026**, *19*, 94908565. https://doi.org/10.26599/NR.2026.94908565

ABSTRACT: Bioelectronics have played a significant role in early detection of cardiovascular and brain diseases under static states. Achieving continuous and high-fidelity dynamic electrophysiological signals monitoring is equally important for evaluation of health conditions during sports. However, the current electrodes for bioelectronics face great challenges of severe motion artifacts caused by low-frequency mechanical vibrations during dynamic body movements. In addition, these electrodes may suffer serious interface separation with skin under dynamic skin deformation that can cause signal disruption. Here, a damping and adhesive hydrogel (DAH) electrode was developed by integrating bovine serum albumin (BSA), amylopectin (AP), and glycerol. Extensive hydrogen bond interactions between BSA and AP endow the DAH with unique viscoelasticity and excellent damping capacity, enabling selective filtering of low-frequency environmental noise. The highly branched structure of amylopectin exposes abundant hydroxyl groups that form strong electrostatic interactions and hydrogen bonds with skin and provides superior adhesiveness. This DAH electrode can maintain high fidelity and signal continuity during various dynamic occasions including walking, tapping and vibration. Based on the DAH, a dynamic robot synchronous control system is demonstrated. Compared with current bioelectronic electrodes, the DAH provides suppressed motion artifact and anti-interface separation ability during dynamic electrophysiological monitoring. Such a DAH could enable the development of next-generation dynamic bioelectronic electrodes.

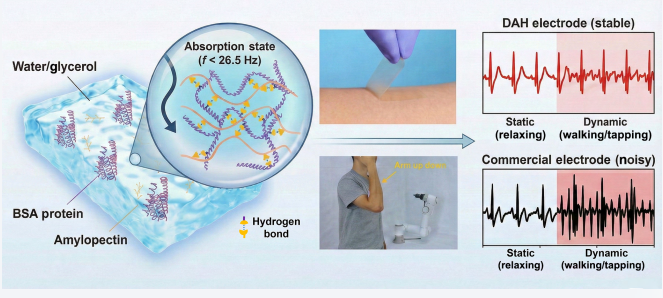

KEYWORDS: electrophysiological monitoring, human–machine interaction, bioelectronics, hydrogel

1 Introduction

Bioelectronics can monitor physiological signals generated from human activity [1–5], playing a significant role in early discovery and diagnosis of different diseases in cardiovascular, muscle, and brain. While current electrophysiological monitoring through bioelectronic electrodes under static conditions has successfully provided valuable physiological information [6–10]. Achieving continuous, stable, and high-fidelity monitoring during dynamic activity is also crucial for real-time assessment of sports conditions. However, dynamic electrophysiological monitoring still faces two primary challenges. First, during activities such as running, tapping, or even deep breathing, electrodes are prone to motion artifacts caused by muscle contractions and low-frequency mechanical vibrations which is mainly distributed between 0.1–30 Hz [11–14]. These interferences significantly reduce the signal-to-noise ratio and compromise monitoring accuracy. Second, significant skin strain and deformation during dynamic movement can easily cause electrode detachment [15–18], leading to severe interface separation and disruption of signal continuity. Therefore, the development of bioelectronic electrodes that simultaneously address both motion artifacts and interface separation is essential and promising for dynamic electrophysiological monitoring.

Several strategies have been proposed to suppress motion artifacts during dynamic electrophysiological monitoring. For example, high-pass filters can reduce mechanical vibration noise but indiscriminately remove real signals [19–21], resulting in signal

Received: December 16, 2025; **Revised:** February 8, 2026
Accepted: February 12, 2026

✉Address correspondence to ymao@zzu.edu.cn

distortion. Machine learning-based methods can remove motion artifact by training classifiers on labeled clean and artifact-contaminated data [22–24], yet they often require high computational complexity. Microneedle electrodes can enhance anti-artifact by improving skin contact [25–27], but their use may raise concerns regarding biocompatibility. Materials with intrinsic damping properties can actively filter low-frequency noise [28–30], offering structural simplicity and high filtering precision, but they still face interface separation issues during dynamic motion. Introducing adhesiveness into electrodes provides a potential solution to prevent interface separation. Catechol-based systems inspired by mussel adhesion, establish hydrogen bonds with substrates to gain high adhesiveness [31–33], but catechol groups are easily oxidized, limiting long-term stability. Biomimetic microstructures such as octopus-inspired suction cups enhance adhesion through physical interlocking [34–36], though they often require complex fabrication. Alternatively, natural polysaccharides such as amylopectin obtained from starch-rich grain crops, composed of numerous α-D-glucose units and a highly branched architecture, provide abundant hydroxyl groups that form dense hydrogen bonds with surrounding molecules, imparting high biocompatible adhesiveness [37–39]. Moreover, the hydroxyl groups can form high-density hydrogen-bond networks with amino groups in proteins, mimicking damping mechanisms in cuticular pad of spider [40], where the dynamic formation and rupture of hydrogen bonds induce rheological transitions that effectively dissipate vibrational energy. Therefore, designing electrodes with combined intrinsic damping and adhesive properties is of great significance for achieving high-fidelity, continuous, and stable dynamic electrophysiological monitoring.

Here, we developed a high damping and adhesive hydrogel (DAH) electrode based on biomaterials including bovine serum albumin (BSA), amylopectin (AP), and glycerol. Extensive hydrogen bond interactions between BSA and AP endow the DAH electrode with unique viscoelasticity and excellent damping capacity, enabling effective dissipation of dynamic impacts and selective filtering of low-frequency environmental noise. Meanwhile, the abundant hydroxyl groups in amylopectin form strong electrostatic interactions and hydrogen bonds with skin surface, providing superior adhesiveness. Under dynamic conditions, the DAH can actively filter motion-induced low-frequency noise, maintains firm conformal contact with skin, and enables long-term continuous, high-quality acquisition of dynamic electrocardiogram (ECG) and electromyogram (EMG) signals, with fidelity significantly surpassing that of commercial electrodes. Based on the DAH electrode, we further developed a dynamic human–machine interaction system, allowing precise control of robotic arm coordination under dynamic conditions, enabling high-precision dynamic interactive applications. This biomaterial-based DAH electrode, combining high damping and strong adhesion properties, offers a promising strategy for high-fidelity, continuous, and stable monitoring of dynamic electrophysiological signals.

2 Results and discussion

2.1 Basic structure of the DAH electrode and schematic of its damping mechanism

The DAH mainly consists of all-natural materials, including BSA protein, AP, glycerol, and water. For comparison as a control sample, a pure BSA hydrogel was prepared without AP. Figure 1(a) illustrates the detailed internal molecular structures of the main components of the DAH, the hydroxyl groups of AP, water, as well as glycerol can form an extensive hydrogen bond crosslinking network with the amino and carboxyl groups of BSA. While the protons can transfer through the water molecules along the hydrogen bond network according to the Grotthuss mechanism [41, 42], providing excellent intrinsic proton conductivity for the DAH. The high-density hydrogen bond network between the BSA and AP molecular chains also endows the DAH with superior damping properties. Due to the branched architecture of the AP provides rich hydroxyl groups that promotes Van der Waals interactions or hydrogen bonding with surrounding substrates, resulting in high adhesiveness of the DAH. As shown in Fig. 1(b), dynamic mechanical analysis was performed on the DAH and pure BSA samples over a frequency range of 1–100 Hz to characterize their damping properties. It can be seen that the modulus increases with the frequency, and the damping factor tanδ of the DAH reaches the maximum value of 2.66 at the frequency of 26.5 Hz, while that of the pure BSA sample is only 0.28 (see Fig. S1 in the Electronic Supplementary Material (ESM)), indicating the transition frequency at 26.5 Hz and much stronger damping ability of the DAH originated from the extensive hydrogen bonds between BSA and AP molecules. The damping material undergoes viscous damping below the transition frequency. When the frequency is higher than transition frequency, tanδ quickly drops down and the modulus dramatically increases with frequency, resulting in a glassy state, enabling elastic transmission of the vibration. The damping mechanism is mainly attributed to the viscoelastic properties of the DAH, which is based on the relaxation time of the damping material. For the viscoelastic properties of the material, the ratio of relaxation time to deformation time is defined as De. When the DAH is in a relaxed state, extensive hydrogen bonds exist between the BSA and AP molecular chains, as shown in Fig. 1(c)(i). As a low-frequency stimulus vibration approaches the DAH, the hydrogen bonds partially break to absorb the vibration energy, which is called a rubbery state, as shown in Fig. 1(c)(ii). If a stimulus vibration with a low frequency (< 26.5 Hz) reaches, relaxation time is shorter than the vibration period (De < 1, viscous), the mechanical stress can recover ahead of next vibration period, thus the vibration energy is absorbed, which is defined as an absorption state. While a vibration stimulus with a frequency higher than 26.5 Hz, the relaxation time is longer than the vibration period (De > 1, elastic), indicating that the stress can recover before the next vibration, which will pass through as the chains rearrange (transmission state), as shown in Fig. 1(c)(iii). Figure 1(d) further shows the young's modulus curve which indicates that the DAH possesses a viscoelastic property, it experiences a phase transition from rubbery to glassy state upon applying a 26.5 Hz of frequency. The phase change enables the DAH to selectively dampen the low-frequency noise under 26.5 Hz and transmit higher-frequency vibration signals, which can be used in filtering dynamic noise under 26.5 Hz. In daily life, the background noise comes from many mechanical body movement sources, such as gait motion, respiration, and blood pressure. The background noise is mainly distributed between 0.1 to 30 Hz, which may cause severe interference with normal electrophysiological signals, as shown in Fig. 1(e). As a result, the current electrodes face great challenges of serious signal artifacts in dynamic electrophysiological acquisition caused by breathing, walking, taping, and running. Therefore, our DAH electrode can selectively

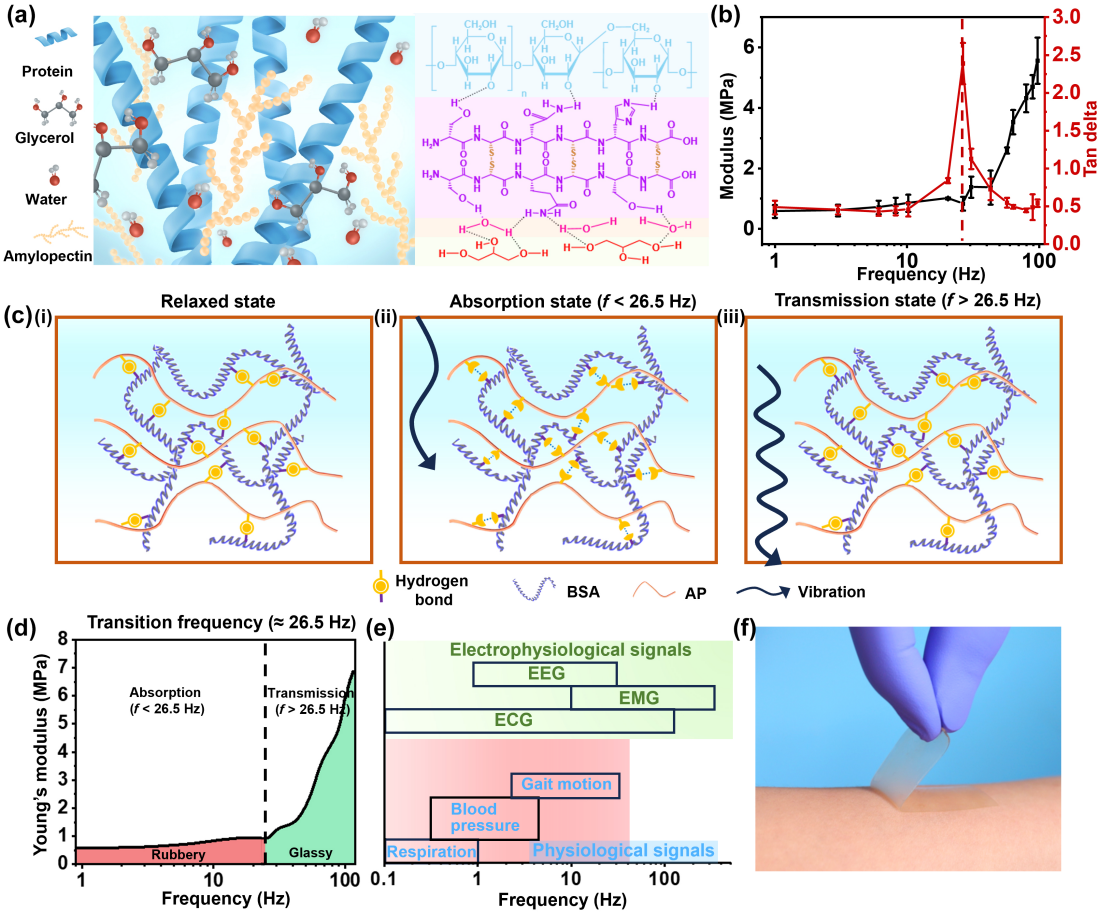

Figure 1 (a) Basic structure and damping mechanism of the DAH. (a) Molecular structures of different components in the DAH. (b) Dynamic mechanical Young's modulus and tanδ of the DAH as a function of frequency. (c) Selective damping mechanism in the DAH showing the transition from absorption state to transmission state. (d) Viscoelastic properties of the DAH showing a rubber-glass transition versus the applied frequency of vibration. (e) Frequency ranges of human physical motion (bule) and electrophysiological (green) signals, as well as the damping frequency range (red) of the DAH electrode. (f) Photograph showing the DAH electrode firmly attached to the arm skin.

absorb the dynamic noise below 26.5 Hz, which can maintain high fidelity during daily exercise dynamic electrophysiological recording. Figure 1(f) presents that the DAH electrode is firmly adhered to the arm skin, indicating its excellent conformability and adhesiveness.

2.2 Mechanical, adhesive and electrical properties of the DAH electrode

The DAH was formed through extensive hydrogen bond crosslinking between amino and carboxyl groups of BSA and hydroxyl groups of AP molecular chains, which endows the DAH with superior mechanical and electrical property. To investigate the influence of amylopectin content on the mechanical properties of the DAH, the stress-strain test was conducted on hydrogel samples with varying content of amylopectin, as shown in Fig. 2(a). It can be seen that as the AP content increases from 0 wt.% to 7.7 wt.%, the elongation at break rises from 360% to the maximum of 655%, while it quickly drops to 420% with the AP further increase to 8.9%. This decline may be attributed to excessive amylopectin concentration tend to self-associate and induce microphase separation, which leads to stress concentration and weaken the tensile elongation. Figure 2(b) extracts the Young's modulus and elongation with changing AP content, the modulus gradually drops from 243 to 88 kPa, demonstrating a matched modulus with human skin and tissues (50–600 kPa). The stress-strain plot of the pure BSA hydrogel sample is presented in Fig. S2 in the ESM, the pure BSA hydrogel exhibits much higher modulus of 1.04 MPa and lower elongation of 485%, further indicating the advantages of the AP modified DAH for epidermal electrodes. Due to the amylopectin's bushy molecular shape with excessive hydroxyl groups which promotes Van der Waals interactions as well as hydrogen bonding with surrounding substrates, the DAH possesses superior adhesiveness. The shear-stress test was performed to test the adhesiveness. The DAH was adhered between two porcine skins, and a shear force was applied to the two porcine skins, the sketch of the experimental setup is depicted in Fig. S3 in the ESM. Figure 2(c) presents the adhesion strength of the DAH with the change of AP content. The adhesion strength reaches the maximum value from 1.1 to 15.6 kPa as AP content increases from 0 wt.% to 7.7 wt.%, then it decreases to 11.7 kPa as the AP content further increases to 8.9 wt.% due to declined stretchability of the hydrogel, confirming that the AP contributes greatly to the adhesiveness due to the rich hydroxyl groups that form a great number of hydrogen bonds with skin surfaces. Figure 2(d) shows the adhesion strength on porcine skin with the rise of glycerol content. The adhesion strength gradually increases with the glycerol content to 15.6 kPa when the glycerol reaches 12.8 wt.%. The increased glycerol would spread on the surface of the hydrogel and

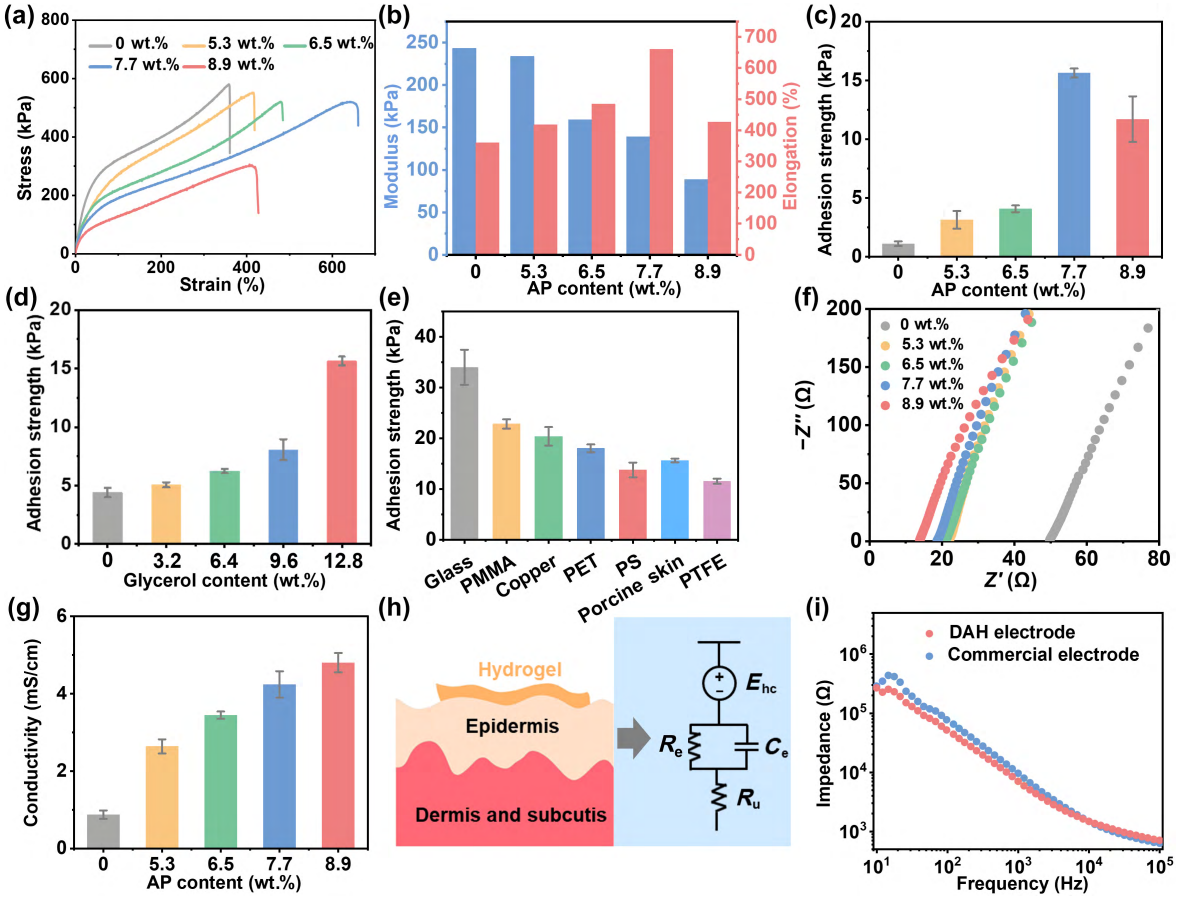

Figure 2 Mechanical and electrical properties of the adhesive DAH. (a) Stress–strain curves of the DAH with different AP contents. (b) Young's modulus and elongation of the DAH with different AP contents. (c) Adhesion strength of the DAH with different AP contents on porcine skin. (d) Adhesion strength of the DAH with different glycerol contents on porcine skin. (e) Adhesion strength of the DAH with optimal formula on various substrates. (f) EIS plots of the DAH with different AP contents. (g) Conductivity of the DAH with different AP contents obtained from the EIS plots. (h) Schematic illustration of the hydrogel adhered on skin and equivalent circuit model for contact impedance measurement. (i) Contact impedance curves of the DAH electrode and commercial electrode over the frequency range of 10 to 10^5 Hz.

increase the density of hydroxyl group on the hydrogel surface, which can form more hydrogen bonds with external substrates, resulting in the enhancement of the adhesion strength. Therefore, the glycerol content was then fixed at 12.8 wt.% for the following sample tests. Due to rich glycerol content, the DAH also possesses excellent water retention ability, as shown in Fig. S4 in the ESM. After 1 day of storage at 20 °C environment, the DAH remains 97% of the original weight, and can maintain 80% of weight after 7 days, which ensures long-term stability of the DAH. Then various substrates were used to test the adhesion strength, Fig. 2(e) shows the different adhesion strength of the DAH with 7.7 wt.% AP content on glass, PMMA, copper, PET, PS, porcine skin, and PTFE. It can be seen that the DAH exhibits high adhesiveness on most daily used substrates, exceeding 11.5 kPa. This excellent adhesiveness assures the DAH firmly attaches to skin surfaces without delamination during dynamic vibration exercise conditions, enabling continuous collection of dynamic electrophysiological signals. The 90° peeling test on various materials was also performed for further adhesion evaluation in sensing, as shown in Fig. S5 in the ESM. Then the electrochemical impedance spectroscopy (EIS) was performed to evaluate the conductivity of the DAH with various contents of AP. Figure 2(f) presents the Nyquist plots of DAH as a function of AP content. And the conductivity was calculated in Fig. 2(g) following $\sigma = L/SR$, where R refers to hydrogel's bulk resistance that is obtained from the X-axis intercept of EIS plots, S and L are the area and thickness of hydrogel. The conductivity rises from 0.9 to 4.8 mS/cm with increasing of AP content. This may be attributed to the highly branched molecular structure of AP that exposes extensive hydroxyl groups capable of forming dense hydrogen-bonding networks with water molecules, leading to the formation of more conductive channels for proton migration. This conductivity is comparable to the latest reported state-of-art literatures [43–46]. Considering the balance between mechanical and electrical properties, AP content was chosen to be 7.7 wt.% for the following DAH application test. The cyclic tensile test was performed on the DAH by stretching to 90% of strain for 100 cycles, as shown in Fig. S6 in the ESM. The DAH exhibited no obvious fatigue in the cyclic stretching test, indicating its fatigue resistance under long-term dynamic service conditions. Then the DAH was adhered to a porcine skin to test the contact impedance to the skin surface. Figure 2(h) shows the equivalent circuit model for contact impedance measurement when the hydrogel is adhered on skin surface. And Fig. 2(i) presents the impedance plots of the DAH and commercial electrode over a frequency range of 10 to 10^5 Hz. Due to the excellent adhesiveness and conductivity of the DAH, it exhibits lower contact impedance to porcine skin compared with the commercial electrode, showing great advantages for high-fidelity electrophysiological acquisitions.

2.3 Damping and shock energy dissipation abilities of the DAH electrode

The DAH electrode's damping properties and shock energy dissipation abilities were systematically studied. First, a dropping ball test was performed on the DAH with a commercial polydimethylsiloxane (PDMS) film as a control sample to characterize its shock-resistance ability and damping behavior. As shown in Fig. 3(a), a steel ball with a diameter of 22 mm was dropped on different damping materials from a height of 25 cm. The damping materials were placed on a steel plate with an accelerometer mounted beneath the damping material to evaluate the elastic absorption and shock energy reflection, representing the basic damping properties of the materials. Figures 3(b) and 3(c) present the accelerometer signals of different damping materials including the DAH, control sample PDMS, and without damper. Compared with the other two conditions, the DAH exhibits much lower amplitude (0.69 mV) of shock acceleration signal, which is 35% that of the shock signal without damper (1.97 mV), indicating a superior damping effect to weaken the shock energy generated by the steel ball. Whereas the accelerometer shock signals with a PDMS control have a 67% higher amplitude (1.15 mV) than the DAH, indicating much lower damping ability. This excellent damping effect is helpful in absorbing and shielding large mechanical vibration noise under dynamic exercise conditions, facilitating the stable and precise acquisition of dynamic electrophysiological signals. Then, the damping effect during daily application scenario was assessed by integrating the DAH with a liquid metal-based strain sensor and applying mechanical forces with different frequencies during daily usage. The serpentine-structured strain sensor is commonly used in strain sensing [47], its design layout, photograph, and strain sensing performance can be found in Figs. S7–S9 in the ESM. The strain sensor was sandwiched between two DAH films with a thickness of 2 mm, while two PDMS films with the same thickness were used as control damper materials (see Fig. S10 in the ESM). When the hydrogel was adhered to soft skin surface, the hydrogel inevitably encounters mechanical noise originating from skin tension during dynamic body movement occasions. These dynamic noises will introduce a broad frequency range of motion artifacts that interfere with the genuine physiological signals. The DAH electrode's damping ability for the movement-induced noise is significant for stable and

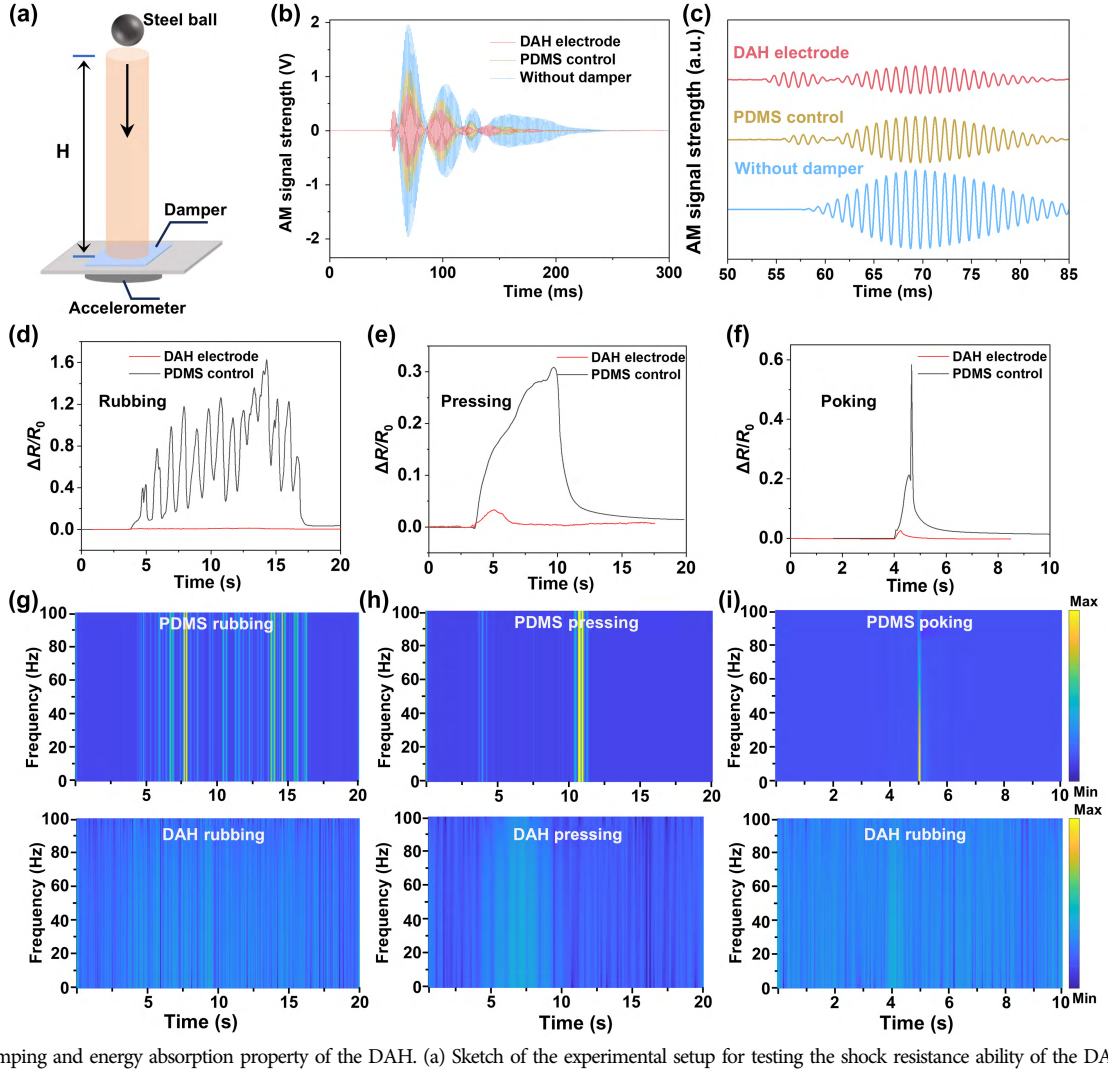

Figure 3 Damping and energy absorption property of the DAH. (a) Sketch of the experimental setup for testing the shock resistance ability of the DAH. (b) and (c) Mechanical vibration signals obtained by an accelerometer under different damping conditions of DAH, PDMS, and without any damper material. Strain variation signals of a strain sensor sandwiched between the DAH and PDMS under different stress states of (d) hand rubbing, (e) finger pressing, and (f) poking. (g)–(i) The corresponding analysis of Morelet wavelet transforms of the damper-integrated strain sensor signals under rubbing, pressing, and poking.

accurate physiological signal acquisition. As demonstrated in Figs. 3(d)–3(f), the integrated strain sensor was applied with rapid skin movement-induced deformation such as pressing, rubbing, and poking. The PDMS sandwiched strain sensor exhibits a dramatic resistance signal variation under the three skin deformation modes, while the DAH-integrated sensor shows a significantly suppressed resistance signal change. The corresponding analysis of Morelet wavelet transforms of the sensor signals of three deformation modes was further performed, as shown in Figs. 3(g)–3(i). The DAH-integrated sensor showed that the low-frequency noise parts caused by mechanical stimulation were dissipated to a large extent, demonstrating a more stable and precise sensor signal. These excellent damping properties of the DAH further demonstrate its advantages in low-motion-artifact dynamic electrophysiological monitoring.

2.4 Dynamic electrophysiological signals monitoring of the DAH electrode

To evaluate the effectiveness of the damping effect in monitoring dynamic electrophysiological signals, the DAH was adhered to various parts of the body to acquire different types of electrophysiological signals during dynamic body motion states. Figure 4(a) shows the DAH electrode adhering to the chest of a young male adult tester for collecting electrocardiogram (ECG) signals. Four types of ECG signals were acquired under different body motion scenarios, including relaxing, stretching, walking, and tapping, as shown in Fig. 4(b). Under every dynamic state, the signals collected by the DAH electrode exhibit stable and clear ECG patterns, whereas those of the commercial Ag/AgCl electrode start to introduce intense background noise and fluctuate to cover the true ECG signals. It is even difficult to distinguish the genuine ECG peaks from the noise under dynamic tapping conditions for the commercial electrode. The sensitivity of ECG electrodes can evaluate the quality of ECG signals, which is defined as the relative voltage ratio of the measured T peak to R peak (T/R value) [48]. Figure 4(c) summarizes the intensity ratio of T/R for the ECG signals acquired by the two electrodes. The DAH exhibits T/R ratio of 0.43, while the commercial electrode is only 0.18 under relaxing state, originating from the high adhesiveness and proton conductivity that decreases the interface impedance. Meanwhile, the

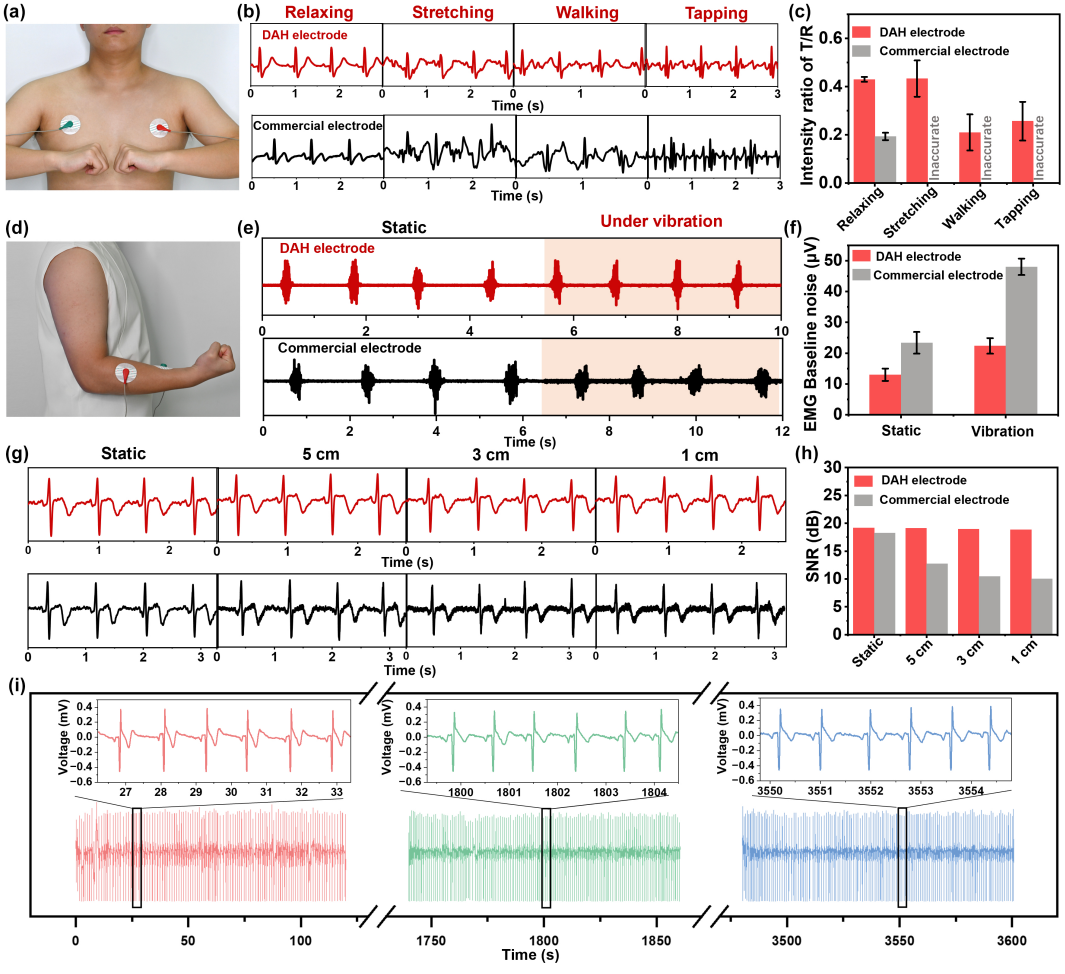

Figure 4 Dynamic electrophysiological monitoring of the DAH electrode. (a) Photograph of the DAH electrode when monitoring dynamic ECG signals. (b) ECG signals acquired by the DAH electrode and commercial electrode under different body conditions including relaxing, stretching, walking, and tapping. (c) The intensity ratio of T/R for the ECG signals acquired by the two electrodes. (d) Photograph of the DAH electrode adhered on arm to collect EMG signals when performing a clenching action. (e) EMG signals acquired by the DAH electrode and commercial electrode under static and mechanical vibration states. (f) Baseline noise of the EMG signals acquired by the two electrodes. (g) ECG signals collected by the DAH electrode and commercial electrode with a vibrator placed at different distances from 1–5 cm to the electrodes. (h) Corresponding signal-to-noise ratio of the ECG signals under different vibration intensities. (i) Long-term uninterrupted dynamic ECG monitoring of the DAH electrode under vibration states for 3600 s.

DAH exhibits a distinguishable T and R peaks during every body movement condition, whereas the commercial electrode can hardly tell the difference in T/R intensity under every dynamic states. This high dynamic fidelity mainly originates from two facts. On one hand, the damping effect of the DAH electrode can actively filter the low-frequency motion artifact in practical dynamic electrophysiological monitoring. Meanwhile, excellent adhesiveness of the DAH can effectively prevent interface separation during dynamic ECG monitoring. Figure 4(d) shows that the DAH electrode was adhered to the arm skin to collect EMG signals when performing a clenching action. A commercial vibrator with a 3 cm distance to electrodes was mounted on the arm skin to exert vibration noise on the arm to simulate a dynamic testing condition. The EMG signals of clenching under static and vibration states were recorded by the DAH and commercial Ag/AgCl electrode respectively, as presented in Fig. 4(e), all showing clear clenching action potentials. Figure 4(f) further extracts the EMG baseline noise collected from the DAH and commercial electrode. It can be seen that the DAH shows 79% lower baseline noise than the commercial electrode under the static state, which is originated from the high proton conductivity of the DAH. Notably, the baseline noise of the DAH gets 115% lower than that of the commercial electrode under strong vibration states, further demonstrating the excellent background noise absorption and anti-interface-separation ability of the DAH. Besides, the DAH can also accurately differentiate finger tiny bending actions as well as the dynamic EMG signals under various grip strengths, as presented in Figs. S11 and S12 in the ESM. Then ECG signals under varying vibration intensities were collected with the vibrator placed at different distances from the electrodes, as presented in Fig. 4(g). The signal-to-noise ratio was extracted accordingly in Fig. 4(h). The signals acquired by DAH presents relatively stable high SNR under various vibration intensities as a result of vibration energy reflection effect and adhesion strengthened interface stability. Whereas the commercial electrode experiences a dramatic SNR drop by 47% with vibrator distance increasing from 5 to 1 cm. To test the long-term stability in dynamic electrophysiological monitoring, the ECG signals with a 1 cm vibration were collected for uninterrupted one hour, as shown in Fig. 4(i). The ECG signals were stable and showed clear P, Q, R, T peaks throughout the dynamic testing period. Owing to the noise-damping ability and excellent adhesiveness, the DAH can effectively eliminate motion artifacts and prevent interface separation compared to traditional commercial electrodes, exhibiting a high-fidelity and high-stability dynamic electrophysiological signal acquisition capability.

2.5 Application of DAH electrode in dynamic human–machine interaction for synchronous robot control

The stable and high-fidelity dynamic electrophysiological signals acquisition performance of the DAH enables it to be applied in dynamic human–machine interaction system for synchronous robot control. As illustrated in Fig. 5(a), various dynamic motion-generated dynamic EMG signals are accurately collected by the DAH and further used to synchronously control a robotic arm. The dynamic robotic control system is composed of a signal acquisition unit, a voltage comparator, and a microcontroller for data processing. The DAH electrodes were adhered to the arm skin to acquire various dynamic hand motion EMG signals. Figure 5(b) show the dynamic EMG signal patterns corresponding to subtle wrist up and down flexion, and large-amplitude arm up–down and left–right bending movements under dynamic jogging state. It can be seen that the signals show stable and highly distinguishable hand motion-generated peaks under dynamic jogging. Figures 5(c) and 5(d) exhibit the corresponding average peak characteristics of the four hand motion signals, showing great difference in both peak amplitude and duration time, which can be extracted for different robotic motion controlling. Then the dynamic EMG signals acquired by the DAH were processed by the voltage comparator and transformed into square wave signals, which were then processed by a microcontroller into machine-readable commands in real time. The robotic arm can thus be controlled to perform both the subtle wrist flexion (Figs. 5(e) and 5(f)) and large arm bending actions (Figs. 5(g) and 5(h)) synchronously along with the human hand motion, also can be seen in Videos S1 and S2 in the ESM. Under dynamic exercise state, the robotic arm can be instantly and precisely controlled without any erroneous actions, demonstrating the excellent dynamic motion recognition accuracy of the DAH in dynamic human–machine interaction applications.

3 Conclusion

In summary, we developed a DAH electrode by integrating natural biomaterials BSA, AP, and glycerol. In the hydrogel structure, the extensive hydrogen bonds between BSA and AP offer unique viscoelasticity and excellent damping capacity that actively absorbs low-frequency mechanical vibration, and abundant hydroxyl groups in the branched AP endow high adhesion to the skin. The DAH also possesses high proton conductivity and water retention ability due to the presents of BSA and glycerol. It exhibits excellent shock energy dissipation and mechanic vibration filtering ability, higher SNR and lower baseline noise when monitoring ECG and EMG signals than the commercial electrodes. The DAH is able to acquire high-fidelity and long term continuous electrophysiological signals during dynamic body motions. Based on the high-quality dynamic EMG signals acquired by the DAH electrode, we further developed a dynamic robot synchronous control system. Compared with commercial bioelectrodes, this DAH electrode can actively remove motion artifacts and prevent interface separation on various dynamic electrophysiological monitoring occasions. This materials design strategy could bring great opportunities to the next generation bioelectrodes for low motion artifact as well as interface-stable dynamic electrophysiological monitoring.

4 Experimental section

4.1 Preparation of the DAH electrode

First, AP was mixed with deionized water at a mass ratio of 5:1 and stirred in an oil bath at 90 °C for 4 h until a viscous, transparent gel-like liquid was formed (referred to as Solution 1). Afterwards, trifluoroethanol (TFEA) and deionized water were mixed at a 1:1 mass ratio in a beaker, followed by the addition of 14 wt.% BSA. The mixture was stirred for 15 min, after which 6 wt.% β-mercaptoethanol was added and thoroughly mixed until a clear solution was obtained (referred to as Solution 2). Subsequently, 5 wt.% of ethylenediamine was mixed with anhydrous ethanol at a 1:1 mass ratio, and the mixture was slowly added to Solution 2 under continuous stirring. After thorough mixing, 12.8 wt.% glycerol was introduced and stirred uniformly to obtain Solution 3. Finally, Solution 3 was thoroughly mixed with Solution 1 to form a viscous liquid. The obtained mixture was cast into a glass dish and uniformly spin-coated at a speed of 300 rad/s. After drying at room

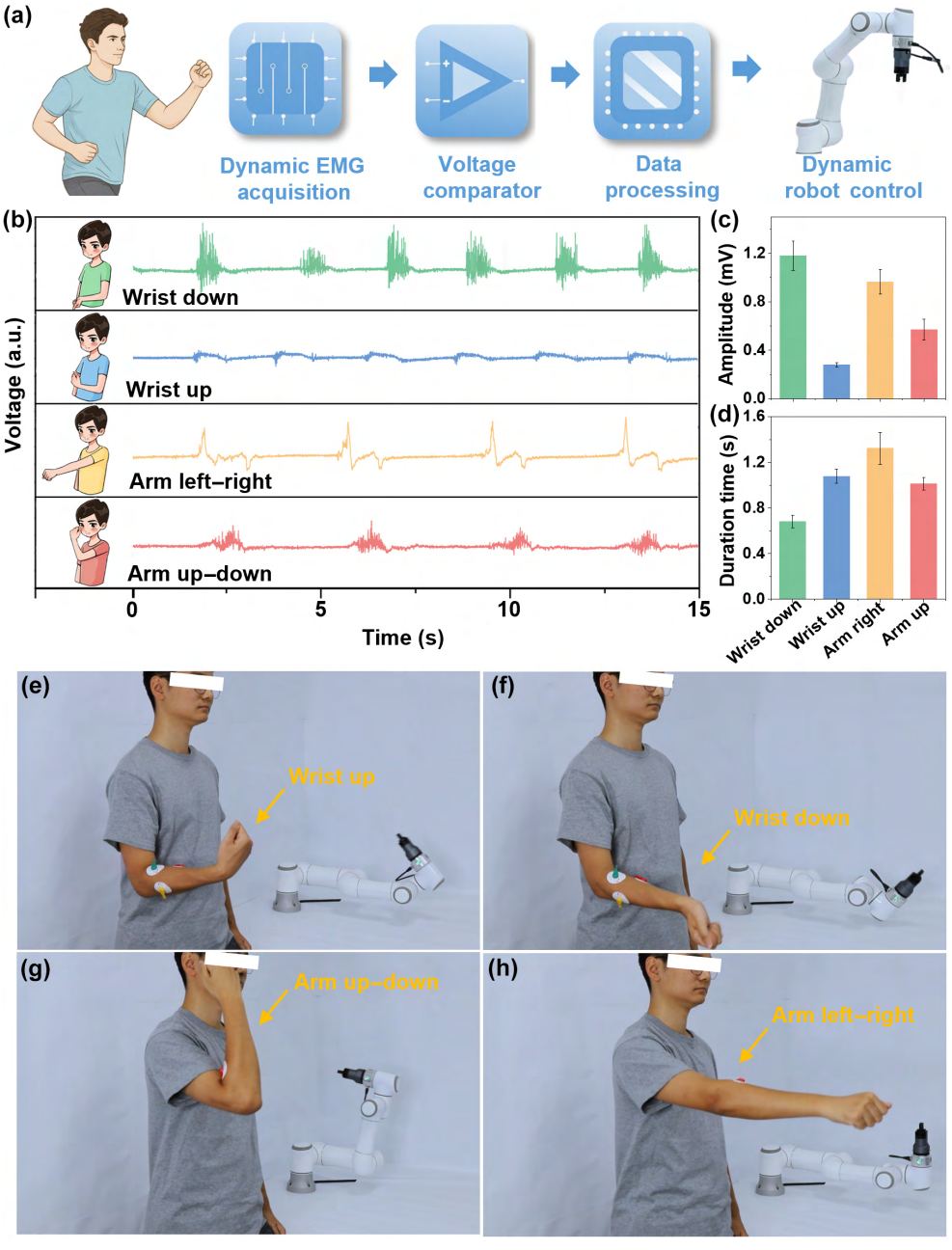

Figure 5 Application of the DAH electrode in a dynamic robot synchronous control system. (a) Schematic illustration of the working process of the robot control system by dynamic EMG signals acquired by the DAH electrode. (b) Dynamic EMG signal patterns corresponding to subtle wrist up and down flexion and large-amplitude arm up–down and left–right bending movements under dynamic jogging state. (c) Average signal amplitude of EMG signals of the four types of hand movements. (d) Average time duration of EMG signals of the four types of hand movements. (e) and (f) Photographs of the dynamic robot synchronous control of wrist up and wrist down flexion movements. (g) and (h) Photographs of the dynamic robot synchronous control of arm up–down and left–right bending movements.

temperature, a hydrogel film with high damping, adhesiveness, and proton conductivity was obtained. The pure BSA hydrogel was prepared according to previously reported literature [49].

4.2 Preparation of the liquid metal-based strain sensor

The PDMS elastomer base and crosslinking agent with 10:1 volume ratio was mixed and spin-coated on a glass substrate, then it was cured at 70 °C for 4 h to obtain a PDMS film with 500 μm thickness. Then a patterned mask with serpentine structure was covered on the PDMS film, the EGaIn liquid metal was screen-coated on the PDMS. Then the mask was removed and two copper leads were connected to two ends of the liquid metal line. The uncured PDMS mixture was spin-coated on the patterned liquid metal. After the PDMS was fully cured, a liquid metal-based strain sensor was obtained.

4.3 Characterization and measurement

The tensile stress-strain curves were tested by a Mark-10 mechanical testing system. An electrochemical workstation (Zahner IM6) was used to perform the impedance tests, and two stainless steel electrodes were used to sandwich the samples. The AC impedance was tested from 4 MHz to 1 Hz with a 10 mV applied

bias. The damping property of the hydrogel was measured by a dynamic mechanical analysis at stretching working mode under varying frequency of 1–100 Hz. The adhesion strength of the DAH was measured by a lap-shear testing method on the Mark-10 tensile testing machine. The DAH was adhered between various substrates with an adhesion area of 20 mm × 20 mm. A dropping ball test (steel ball diameter 22 mm, dropping height 25 cm) was used to test the energy dissipation ability of the DAH, an accelerometer (WT-VB01-485, WitMotion Shenzhen Co., Ltd) was placed under the damping material to measure dampened shock energy. The ECG test was performed on a heart and brain SpikerBox device (Backyard Brains). The EMG signals were acquired by using a recording toolkit (Muscle SpikerShield Pro). The EEG test was conducted on a biomedical signal acquisition system. Different extent of vibration was applied during the EMG and ECG tests by attaching a commercial vibrator (RISYM, WEIXIN electronics) to the skin at varying distances to the electrodes.

Electronic Supplementary Material: Supplementary material (dynamic mechanical analysis of the BSA hydrogel, stress–strain curves of the BSA hydrogel and DAH electrode, schematic illustration of the lap shear test, weight change plot of the DAH electrode during storage, design layout and photograph of the liquid metal-based strain sensor, schematic diagram to test the vibration damping effect of the DAH electrode, EMG signals of different finger's tiny bending actions captured by DAH electrode, and amplitude of different finger's bending generated EMG signals) is available in the online version of this article at https://doi.org/10.26599/NR.2026.94908565.

Data availability

All data needed to support the conclusions in the paper are presented in the manuscript and the Electronic Supplementary Material. Additional data related to this paper may be requested from the corresponding author upon request.

Acknowledgments

This work was supported by the National Natural Science Foundation of China (No. 12504040), Henan Province Science and Technology Research and Development Program Joint Fund Advantageous Discipline Cultivation Project (No. 232301420033), and Innovation Training Program for College Students of Zhengzhou University (Nos. 202510459147 and 202510459058).

Declaration of competing interest

All the contributing authors report no conflict of interests in this work.

Author contribution statement

P. C. Z.: Project administration, writing manuscript, experimental design. Y. T. Z.: Data curation, validation. A. B. W.: Data curation. Y. X. F.: Investigation. Y. M. L.: Investigation. M. J. N.: Data curation. N. N. H.: Data curation, experimental design, Y. Y. L.: Investigation. Z. F. P.: Validation. Y. C. M.: Funding acquisition, project administration, experimental design, review & editing manuscript. All the authors have approved the final manuscript.

Use of AI statement

None.

References

[1] Xie, R. J.; Han, F.; Yu, Q. H. Y.; Li, D.; Han, X.; Xu, X. L.; Yu, H.; Huang, J. P.; Zhou, X. M.; Zhao, H. et al. A movable long-term implantable soft microfibre for dynamic bioelectronics. *Nature* **2025**, *645*, 648–655.

[2] Kasuba, K. C.; Buccino, A. P.; Bartram, J.; Gaub, B. M.; Fauser, F. J.; Ronchi, S.; Kumar, S. S.; Geissler, S.; Nava, M. M.; Hierlemann, A. et al. Mechanical stimulation and electrophysiological monitoring at subcellular resolution reveals differential mechanosensation of neurons within networks. *Nat. Nanotechnol.* **2024**, *19*, 825–833.

[3] Yu, S. F.; Ji, Z. Z.; Liu, L.; Huang, Z. J.; Luo, Y. H.; Wang, H. S.; Wangyuan, R.; Guo, Z. Q.; Chen, Z.; Liao, Q. L. et al. A hyperconformal dual-modal metaskin for well-defined and high-precision contextual interactions. *Nat. Commun.* **2025**, *16*, 10573.

[4] Yan, Z. C.; Xu, D.; Lin, Z. Y.; Wang, P. Q.; Cao, B. C.; Ren, H. Y.; Song, F.; Wan, C. Z.; Wang, L. Y.; Zhou, J. X. et al. Highly stretchable van der Waals thin films for adaptable and breathable electronic membranes. *Science* **2022**, *375*, 852–859.

[5] Li, Y.; Gu, Y. Z.; Qian, S.; Zheng, S. W.; Pang, Y. C.; Wang, L. L.; Liu, B. G.; Liu, S. J.; Zhao, Q. An injectable, self-healable, and reusable PEDOT:PSS/PVA hydrogel patch electrode for epidermal electronics. *Nano Res.* **2024**, *17*, 5479–5490.

[6] Chen, B. J.; Yu, R. J.; Wang, J. Q.; Feng, Y. X.; Zhang, Y. J.; Mao, Y. C.; Shan, C. X.; Wang, X. D. Biomaterials-based hydrogel with superior bio-mimetic ionic conductivity and tissue-matching softness for bioelectronics. *Adv. Funct. Mater.*, in press, DOI: 10.1002/adfm.202527495.

[7] Deuschl, G.; Becktepe, J. S.; Dirkx, M.; Haubenberger, D.; Hassan, A.; Helmich, R. C.; Muthuraman, M.; Panyakaew, P.; Schwingenschuh, P.; Zeuner, K. E. et al. The clinical and electrophysiological investigation of tremor. *Clin. Neurophysiol.* **2022**, *136*, 93–129.

[8] Page, S. C.; Sripathy, S. R.; Farinelli, F.; Ye, Z. Y.; Wang, Y. H.; Hiler, D. J.; Pattie, E. A.; Nguyen, C. V.; Tippani, M.; Moses, R. L. et al. Electrophysiological measures from human iPSC-derived neurons are associated with schizophrenia clinical status and predict individual cognitive performance. *Proc. Natl. Acad. Sci. USA* **2022**, *119*, e2109395119.

[9] Tatum IV, W. O. Long-term EEG monitoring: A clinical approach to electrophysiology. *J. Clin. Neurophysiol.* **2001**, *18*, 442–455.

[10] Zhu, P. C.; Niu, M. J.; Liang, S. Y.; Yang, W. Q.; Zhang, Y. T.; Chen, K.; Pan, Z. F.; Mao, Y. C. Non-hand-worn, load-free VR hand rehabilitation system assisted by deep learning based on ionic hydrogel. *Nano Res.* **2025**, *18*, 94907301.

[11] Zhao, Y.; Zhang, S.; Yu, T. H.; Zhang, Y.; Ye, G.; Cui, H.; He, C. Z.; Jiang, W. C.; Zhai, Y.; Lu, C. M. et al. Ultra-conformal skin electrodes with synergistically enhanced conductivity for long-time and low-motion artifact epidermal electrophysiology. *Nat. Commun.* **2021**, *12*, 4880.

[12] Kline, J. E.; Huang, H. J.; Snyder, K. L.; Ferris, D. P. Isolating gait-related movement artifacts in electroencephalography during human walking. *J. Neural Eng.* **2015**, *12*, 046022.

[13] Sweeney, K. T.; Ward, T. E.; McLoone, S. F. Artifact removal in physiological signals-practices and possibilities. *IEEE Trans. Inf. Technol. Biomed.* **2012**, *16*, 488–500.

[14] Yin, J. Y.; Wang, S.; Tat, T.; Chen, J. Motion artefact management for soft bioelectronics. *Nat. Rev. Bioeng.* **2024**, *2*, 541–558.

[15] He, C. B.; Zhang, J.; Wang, H. F.; Wu, D.; Zheng, H. Y.; Guo, Z. N.; Xie, J.; Zhu, W. H.; Xie, M. Y.; Zhong, J. et al. Accurate and reliable detection of dynamic electrophysiological signals via *in situ* formation of epidermal electrodes. *Adv. Funct. Mater.* **2026**, *36*, e09372.

[16] Li, H. F.; Zhao, H.; Song, K. K.; Han, F.; Liu, Z. Y.; Tian, Q. Flexible and stretchable implantable devices for peripheral neuromuscular electrophysiology. *Nanoscale* **2024**, *16*, 6402–6428.

[17] Zhou, N. J.; Ji, J. J.; Qu, R. X.; Feng, X.; Song, X. K.; Chen, M. J.; Chen, F. G.; Ma, Z. J.; Wei, Y. Permeable and durable liquid-metal fiber mat as implantable physiological electrodes with long-term biocompatibility. *Adv. Mater.* **2025**, *37*, 2413728.
[18] Cheng, Y.; Zhou, Y.; Wang, R. R.; Chan, K. H.; Liu, Y.; Ding, T. P.; Wang, X. Q.; Li, T. T.; Ho, G. W. An elastic and damage-tolerant dry epidermal patch with robust skin adhesion for bioelectronic interfacing. *ACS Nano* **2022**, *16*, 18608–18620.
[19] Gómez-Echavarría, A.; Ugarte, J. P.; Tobón, C. The fractional Fourier transform as a biomedical signal and image processing tool: A review. *Biocybern. Biomed. Eng.* **2020**, *40*, 1081–1093.
[20] Lin, C. F.; Zhu, J. D. Hilbert-Huang transformation-based time-frequency analysis methods in biomedical signal applications. *Proc. Inst. Mech. Eng. H* **2012**, *226*, 208–216.
[21] Ranjan, R.; Sahana, B. C.; Bhandari, A. K. Motion artifacts suppression from EEG signals using an adaptive signal denoising method. *IEEE Trans. Instrum. Meas.* **2022**, *71*, 1–10.
[22] Sun, W. T.; Su, Y. P.; Wu, X.; Wu, X. J. A novel end-to-end 1D-ResCNN model to remove artifact from EEG signals. *Neurocomputing* **2020**, *404*, 108–121.
[23] Lim, J.; Hajeb, S.; Kong, Y. S.; Chon, K. H. Deep learning for suppressing EMG and motion artifacts in armband ECG R-peak detection. *Biomed. Eng. Lett.* **2026**, *16*, 29–40.
[24] Mahmud, S.; Hossain, M. S.; Chowdhury, M. E. H.; Reaz, M. B. I. MLMRS-Net: Electroencephalography (EEG) motion artifacts removal using a multi-layer multi-resolution spatially pooled 1D signal reconstruction network. *Neural Comput. Appl.* **2023**, *35*, 8371–8388.
[25] Ji, H. W.; Wang, M. Y.; Wang, Y. T.; Wang, Z. H.; Ma, Y. J.; Liu, L. L.; Zhou, H. L.; Xu, Z.; Wang, X.; Chen, Y. et al. Skin-integrated, biocompatible, and stretchable silicon microneedle electrode for long-term EMG monitoring in motion scenario. *npj Flex. Electron.* **2023**, *7*, 46.
[26] Krieger, K. J.; Lijnse, T. M.; Lowery, M. M.; O'Cearbhaill, E. D. Microneedle electrodes for electromyography. *Biosens. Bioelectron.* **2025**, *290*, 117945.
[27] Ren, L.; Liu, B.; Zhou, W.; Jiang, L. L. A mini review of microneedle array electrode for bio-signal recording: A review. *IEEE Sens. J.* **2020**, *20*, 577–590.
[28] Huang, J. R.; Chen, A. B.; Liao, J. R.; Han, S. J.; Wu, Q. R.; Zhang, J. Y.; Chen, Y. J.; Lin, X. D.; Guan, L. H. Physiological sensing system integrated with vibration sensor and frequency gel dampers inspired by spider. *Mater. Horiz.* **2024**, *11*, 822–834.
[29] Xu, Z. Y.; Lu, J. J.; Lu, D.; Li, Y. R.; Lei, H.; Chen, B.; Li, W. F.; Xue, B.; Cao, Y.; Wang, W. Rapidly damping hydrogels engineered through molecular friction. *Nat. Commun.* **2024**, *15*, 4895.
[30] Zhao, J. H.; Li, M.; Chen, J. W.; Gao, W. W.; Bai, H. Energy-absorbing porous materials: Bioinspired architecture and fabrication. *Nano Res.* **2024**, *17*, 679–690.
[31] Zhang, C.; Zhou, Y. S.; Han, H. J.; Zheng, H. X.; Xu, W. H.; Wang, Z. K. Dopamine-triggered hydrogels with high transparency, self-adhesion, and thermoresponse as skinlike sensors. *ACS Nano* **2021**, *15*, 1785–1794.
[32] Lancelot, A.; Meger, M. E.; Guerreiro Gómez, E.; Sierra, T.; Wilker, J. J. Adhesion of catechol-functionalized linear-dendritic block copolymers: Dendritic effect, self-assembly, and bioadhesion. *Adv. Funct. Mater.* **2025**, *35*, 2413398.
[33] Du, S.; Zhou, N. Y.; Gao, Y. J.; Xie, G.; Du, H. Y.; Jiang, H.; Zhang, L. B.; Tao, J.; Zhu, J. T. Bioinspired hybrid patches with self-adhesive hydrogel and piezoelectric nanogenerator for promoting skin wound healing. *Nano Res.* **2020**, *13*, 2525–2533.
[34] Fang, Y. L.; Xiong, X. H.; Yang, L.; Yang, W. Y.; Wang, H.; Wu, Q.; Liu, Q. W.; Cui, J. X. Phase change hydrogels for bio-inspired adhesion and energy exchange applications. *Adv. Funct. Mater.* **2023**, *33*, 2301505.
[35] Kim, J.; Yeom, J.; Ro, Y. G.; Na, G.; Jung, W.; Ko, H. Plasmonic hydrogel actuators for octopus-inspired photo/thermoresponsive smart adhesive patch. *ACS Nano* **2024**, *18*, 21364–21375.
[36] Wei, M.; Wu, T.; Lin, B. Y.; Zhou, Q.; Gao, B. B. Two sides in one coin: Emerging biomimetic multistage ordered microstructure-based adhesion and microfluidics. *Sens. Actuators A: Phys.* **2025**, *388*, 116496.
[37] Al Boustani, G.; Xu, Z. R.; Teshima, T. F.; Bichlmaier, L.; Nikić, M.; Hiendlmeier, L.; Sayn-Wittgenstein, A.; Tüzün, D.; Inoue, S.; Wolfrum, B. Non-conductive and conductive washable amylopectin-mastic gum adhesives for on-skin applications. *Adv. Mater. Technol.* **2024**, *9*, 2400719.
[38] Hu, F. H.; Yu, D. H.; Gong, X.; Li, Z. Y.; Zhao, R.; Wang, Q.; Zhang, F. S.; Li, G. D.; Wang, H. L.; Liu, W. X. et al. Amylopectin-enhanced MXene/gallium hydrogels: High-performance flexible conductive materials for multifunctional sensing, EMI shielding, and energy storage applications. *Chem. Eng. J.* **2025**, *510*, 161793.
[39] Zhou, H. W.; Lai, J. L.; Zheng, B. H.; Jin, X. L.; Zhao, G. X.; Liu, H. B.; Chen, W. X.; Ma, A. J.; Li, X. S.; Wu, Y. P. From glutinous-rice-inspired adhesive organohydrogels to flexible electronic devices toward wearable sensing, power supply, and energy storage. *Adv. Funct. Mater.* **2022**, *32*, 2108423.
[40] Park, B.; Shin, J. H.; Ok, J.; Park, S.; Jung, W.; Jeong, C.; Choy, S.; Jo, Y. J.; Kim, T. I. Cuticular pad-inspired selective frequency damper for nearly dynamic noise-free bioelectronics. *Science* **2022**, *376*, 624–629.
[41] Agmon, N. The Grotthuss mechanism. *Chem. Phys. Lett.* **1995**, *244*, 456–462.
[42] Ma, C.; Dong, J. J.; Viviani, M.; Tulini, I.; Pontillo, N.; Maity, S.; Zhou, Y.; Roos, W. H.; Liu, K.; Herrmann, A. et al. De novo rational design of a freestanding, supercharged polypeptide, proton-conducting membrane. *Sci. Adv.* **2020**, *6*, eabc0810.
[43] Han, F.; Chen, S. M.; Wang, F.; Liu, M.; Li, J. H.; Liu, H.; Yang, Y. S.; Zhang, H. Q.; Liu, D.; He, R. Y. et al. High-conductivity, self-healing, and adhesive ionic hydrogels for health monitoring and human–machine interactions under extreme cold conditions. *Adv. Sci.* **2025**, *12*, 2412726.
[44] Li, T.; Qi, H. B.; Zhao, Y. J.; Kumar, P.; Zhao, C. C.; Li, Z. M.; Dong, X. Y.; Guo, X.; Zhao, M.; Li, X. W. et al. Robust and sensitive conductive nanocomposite hydrogel with bridge cross-linking-dominated hierarchical structural design. *Sci. Adv.* **2024**, *10*, eadk6643.
[45] Ji, D.; Park, J. M.; Oh, M. S.; Nguyen, T. L.; Shin, H.; Kim, J. S.; Kim, D.; Park, H. S.; Kim, J. Superstrong, superstiff, and conductive alginate hydrogels. *Nat. Commun.* **2022**, *13*, 3019.
[46] Zhang, Y. X.; Xu, Y. Y.; Wu, C.; Chen, S. Y.; Chen, Z. Y.; Qin, F.; Hu, X. F.; Zhang, J. Y.; Wang, Y. B. Injectable conductive hydrogel patch with spatiotemporally tailored asymmetric adhesion for myocardial infarction repair. *Adv. Mater.* **2026**, *38*, e10824.
[47] Shi, C. Q.; Zou, Z. N.; Lei, Z. P.; Zhu, P. C.; Nie, G. H.; Zhang, W.; Xiao J. J. Stretchable, rehealable, recyclable, and reconfigurable integrated strain sensor for joint motion and respiration monitoring. *Research* **2021**, *2021*, 9846036.
[48] Lai, H. T.; Liu, Y.; Cheng, Y.; Shi, L. J.; Wang, R. R.; Sun, J. Temperature-triggered adhesive bioelectric electrodes with long-term dynamic stability and reusability. *Adv. Sci.* **2023**, *10*, 2300793.
[49] Leng, Z. W.; Zhu, P. C.; Wang, X. C.; Wang, Y. F.; Li, P. S.; Huang, W.; Li, B. C.; Jin, R.; Han, N. N.; Wu, J. et al. Sebum-membrane-inspired protein-based bioprotonic hydrogel for artificial skin and human–machine merging interface. *Adv. Funct. Mater.* **2023**, *33*, 2211056.